UC Office of the President
Recent Work

Title
Constraining cosmology and ionization history with combined 21 cm power spectrum and global signal measurements

Permalink
https://escholarship.org/uc/item/6d22939f

Authors
Liu, Adrian
Parsons, Aaron

Publication Date
2015-12-04

Peer reviewed

Constraining cosmology and ionization history with combined $21\,\mathrm{cm}$ power spectrum and global signal measurements

Adrian Liu,[1,2]⋆† Aaron R. Parsons[1,3]

[1]*Department of Astronomy, University of California Berkeley, Berkeley, CA 94720, USA*
[2]*Berkeley Center for Cosmological Physics, University of California Berkeley, Berkeley, CA 94720, USA*
[3]*Radio Astronomy Laboratory, University of California Berkeley, Berkeley, CA 94720, USA*

30 October 2015

ABSTRACT
Improvements in current instruments and the advent of next-generation instruments will soon push observational 21 cm cosmology into a new era, with high significance measurements of both the power spectrum and the mean ("global") signal of the 21 cm brightness temperature. In this paper we use the recently commenced Hydrogen Epoch of Reionization Array as a worked example to provide forecasts on astrophysical and cosmological parameter constraints. In doing so we improve upon previous forecasts in a number of ways. First, we provide updated forecasts using the latest best-fit cosmological parameters from the *Planck* satellite, exploring the impact of different *Planck* datasets on 21 cm experiments. We also show that despite the exquisite constraints that other probes have placed on cosmological parameters, the remaining uncertainties are still large enough to have a non-negligible impact on upcoming 21 cm data analyses. While this complicates high-precision constraints on reionization models, it provides an avenue for 21 cm reionization measurements to constrain cosmology. We additionally forecast HERA's ability to measure the ionization history using a combination of power spectrum measurements and semi-analytic simulations. Finally, we consider ways in which 21 cm global signal and power spectrum measurements can be combined, and propose a method by which power spectrum results can be used to train a compact parameterization of the global signal. This parameterization reduces the number of parameters needed to describe the global signal, increasing the likelihood of a high significance measurement.

Key words: dark ages, reionization, first stars – methods: data analysis – techniques: interferometric – radio lines: general

1 INTRODUCTION

In coming years, experiments targeting the highly redshifted 21 cm line will transform both astrophysics and cosmology. Large scale cosmological surveys of the 21 cm brightness temperature probe the density, ionization state, and spin temperature of hydrogen atoms in the intergalactic medium (IGM), making them powerful *direct* probes of the reionization epoch, when the first generation of galaxies systematically ionized the IGM. Such measurements promise to place exquisite constraints on the parameters governing these first galaxies that have hitherto been essentially unconstrained (Pober et al. 2014; Greig & Mesinger 2015). 21 cm cosmology

also has the potential to probe the pre-reionization epoch, providing insight into heating mechanisms in our early Universe, whether from X-ray sources (Christian & Loeb 2013, Mesinger et al. 2014; Ewall-Wice et al., submitted), structure formation shocks (Gnedin & Shaver 2004), or exotic phenomena such as dark matter annihilation (Valdés et al. 2013; Evoli et al. 2014). From the standpoint of cosmology, a better understanding of reionization via 21 cm cosmology removes a key nuisance from cosmic microwave background (CMB) datasets, allowing improved constraints on cosmological parameters such as the amplitude of primordial scalar fluctuations (Clesse et al. 2012; Liu et al. 2015). With the 21 cm line potentially capable of accessing larger fractions of our observable Universe than any other cosmological probe, futuristic surveys will not only further refine our limits on fundamental parameters (McQuinn et al. 2006; Mao et al.

⋆ Hubble Fellow
† E-mail: acliu@berkeley.edu

2008; Visbal et al. 2009), but may also provide precision tests of the inflationary paradigm (Cooray et al. 2008; Barger et al. 2009). For reviews of the capabilities of 21 cm cosmology, see e.g. Furlanetto et al. (2006); Morales & Wyithe (2010); Pritchard & Loeb (2012); Loeb & Furlanetto (2013).

Recent years have seen increased experimental activity within 21 cm cosmology. Current observational efforts targeting the reionization epoch can be roughly divided into two categories. Large radio interferometers such as the Murchison Widefield Array (MWA; Tingay et al. 2013; Bowman et al. 2013), the Donald C. Backer Precision Array for Probing the Epoch of Reionization (PAPER; Parsons et al. 2010), the Low Frequency Array (LOFAR; van Haarlem et al. 2013), and the Giant Metrewave Radio Telescope (GMRT; Paciga et al. 2013) aim to measure the spatial fluctuations of the 21 cm brightness temperature field, particularly the power spectrum of these fluctuations. In contrast, smaller scale experiments consisting of single dipole antennas or a small handful of elements seek to characterize the mean 21 cm signal (the "global signal") as a function of redshift (Shaver et al. 1999). Examples of global signal experiments include the Experiment to Detect the Global Epoch of Reionization Signature (EDGES; Bowman & Rogers 2010), the Large-Aperture Experiment to Detect the Dark Ages (LEDA; Greenhill & Bernardi 2012), the Shaped Antenna Measurement of the Background Radio Spectrum (SARA; Patra et al. 2013), the Sonda Cosmológica de las Islas para la Detección de Hidrógeno Neutro (SCI-HI; Voytek et al. 2014), the Zero-spacing Interferometer Measurements of the Background Radio Spectrum (ZEBRA; Mahesh et al. 2014), and the Broadband Instrument for Global Hydrogen Reionization Signal (BIGHORNS; Sokolowski et al. 2015).

Multiple instruments have steadily increased in sensitivity while slowly overcoming foreground contaminants (such as Galactic synchrotron radiation), which are typically more than 10^4 times brighter in temperature than theoretical expectations for the reionization 21 cm signal (Santos et al. 2005; Wang et al. 2006; de Oliveira-Costa et al. 2008). While a positive detection of the cosmological 21 cm signal has yet to be made at the low frequencies corresponding to reionization redshifts (see Masui et al. 2013 and Switzer et al. 2013 for a detection at $z \sim 0.8$ in cross-correlation with galaxy surveys), scientifically interesting limits are beginning to appear. Paciga et al. (2013), Parsons et al. (2014), Dillon et al. (2014), Jacobs et al. (2015), and Dillon et al. (2015) have all set increasingly stringent upper limits on the 21 cm power spectrum, and the current best limits (Ali et al. 2015) have been able to place constraints on IGM heating at $z \sim 8.4$ (Pober et al. 2015; Greig et al. 2015). Global 21 cm signal experiments have shown similar progress, with various published constraints on the strength of the signal (Rogers & Bowman 2008; Bowman et al. 2008; Voytek et al. 2014; Vedantham et al. 2015). The current best published results rule out the possibility of reionization happening more quickly than $\Delta z = 0.06$ (Bowman & Rogers 2010).

Continual improvements in existing instruments (e.g., Mozdzen et al. 2015) and the advent of new instruments make it likely for there to be a positive detection of the cosmological 21 cm signal soon. Beyond a first detection, the proposed Square Kilometer Array (SKA; Mellema et al. 2013) and the recently commenced Hydrogen Epoch of Reionization Array (HERA; Pober et al. 2014) are fore-

casted to characterize the 21 cm power spectrum with high signal-to-noise. New instruments such as the Dark Ages Radio Explorer (DARE; Burns et al. 2012) are similarly being proposed to target the global signal.

With high significance results expected soon from both the power spectrum and global signal experiments, it is timely to re-examine the forecasted performance of upcoming experiments. In this paper, we build on previous forecasting exercises such as Pober et al. (2014) and Greig & Mesinger (2015) and implement a number of improvements in the forecasting methodology. Previous studies have typically kept cosmological parameters fixed while varying the astrophysical parameters that govern reionization. Here, we vary all parameters simultaneously, using HERA as a worked example to see how well these parameters can be constrained by 21 cm power spectrum observations. HERA is a recently commenced next-generation instrument possessing $54,000\,\mathrm{m}^2$ of collecting area, consisting of 331 drift-scanning dishes in a tightly packed hexagonal configuration to maximize sensitivity to the power spectrum. (For more details, see Sec. 2.1). The fiducial parameters used in our forecasts are chosen to match the latest CMB results from the *Planck* satellite (Planck Collaboration et al. 2015a,b). This is in contrast to previous studies, which typically centered their cosmological parameters on the best-fit values from the Wilkinson Microwave Anisotropy Probe (WMAP; Hinshaw et al. 2013). Our updated forecasts thus capture the fact that *Planck* predicts a lower redshift of reionization than WMAP did. We also show how power spectrum measurements can be paired with semi-analytic simulations of reionization to predict the ionization history, and forecast the expected uncertainties within this framework. A special emphasis is placed on how global signal and power spectrum measurements may be combined. We explore the power of joint fits and additionally propose a method for parameterizing the global signal based on power spectrum results.

The rest of this paper is organized as follows. In Sec. 2 we provide our updated forecasts for astrophysical and cosmological parameter constraints, as well as our forecasts for ionization history constraints. Sec. 3 adds global signal measurements to the parameter fits. In Sec. 4 we show how parameter constraints from a power spectrum measurement can be used to construct a parameterization of the global signal that economically accounts for deviations from a fiducial global signal model with only a small handful of parameters. We summarize our conclusions in Sec. 5.

2 UPDATED CONSTRAINTS FROM POWER SPECTRUM MEASUREMENTS

In this section, we briefly update previous forecasts on the parameter estimation performance of upcoming instruments. Using HERA as a worked example, we will emphasize several points. First, we will show that despite the exquisite precision of base ΛCDM parameters from *Planck*, errors on cosmological parameters have a non-negligible impact on parameter forecasts from 21 cm power spectrum measurements. We will also find that while HERA is capable of producing precise parameter constraints over a wide range of reionization scenario, those constraints are markedly more precise if reionization occurs at the lower end of the redshift

range favored by *Planck*. Finally, we will generate forecasts for ionization history constraints based on a HERA measurement of the power spectrum.

2.1 Forecasting methodology

Fitting observational data (grouped here into a vector $\mathbf{d}$) with a model is tantamount to determining the likelihood function $\mathcal{L}(\mathbf{d}, \boldsymbol{\theta})$, which is essentially a probability distribution function for the model parameters (grouped into a vector $\boldsymbol{\theta}$) given the data. Forecasting the performance of an instrument is then roughly equivalent to determining the width of the likelihood function. For speed and simplicity, we perform this forecasting using the Fisher matrix formalism. The Fisher formalism approximates the likelihood function $\mathcal{L}$ as a multi-dimensional Gaussian in the parameters, with the Fisher matrix $\mathbf{F}$ quantifying the curvature of the negative logarithm of the likelihood, i.e.,

$$\mathbf{F}_{\alpha\beta} = -\left\langle \frac{\partial^2 \ln \mathcal{L}}{\partial \theta_\alpha \partial \theta_\beta} \right\rangle, \qquad (1)$$

where θ_α is the αth parameter that we wish to measure, and the angle brackets $\langle \ldots \rangle$ denote an ensemble average over data. It is understood that the derivatives are to be evaluated about fiducial parameter values. The predicted error bar on θ_α about its fiducial value is then given by $(\mathbf{F}^{-1})_{\alpha\alpha}^{1/2}$ if all parameters are fit jointly, and $(\mathbf{F}_{\alpha\alpha})^{-1/2}$ if all other parameters are held fixed. Because the Fisher matrix formalism assumes Gaussian likelihoods, it is an approximation to a full computation of the likelihood (e.g., using Markov Chain Monte Carlo methods). However, the Fisher formalism has the advantage of a much lower computational cost. This is crucial for the present work, for while computations of the full likelihood are feasible if only astrophysical parameters are varied (Greig & Mesinger 2015), here we wish to simultaneously vary cosmological parameters. As long as the error bars are reasonably tight, the Fisher matrix approach should be an excellent approximation.

To compute the Fisher matrix for a measurement of the 21 cm power spectrum, we follow the steps used in Pober et al. (2014). For a power spectrum measurement, Eq. (1) reduces to

$$\mathbf{F}_{\alpha\beta}^{\text{PS}} = \sum_{k,z} \frac{1}{\varepsilon_{\text{PS}}^2(k,z)} \frac{\partial \Delta^2(k,z)}{\partial \theta_\alpha} \frac{\partial \Delta^2(k,z)}{\partial \theta_\beta}, \qquad (2)$$

where the superscript serves to remind us that this pertains to a power spectrum measurement, $\varepsilon_{\text{PS}}(k,z)$ is the error (at spatial wavenumber k and redshift z) on the measurement of $\Delta^2(k,z) \equiv (k^3/2\pi^2)P_{21}(k,z)$, and the power spectrum $P_{21}(k,z)$ is defined as

$$\langle \widetilde{\Delta T}_{21}(\mathbf{k},z)\widetilde{\Delta T}_{21}^*(\mathbf{k}',z)\rangle \equiv (2\pi)^3\delta^D(\mathbf{k}-\mathbf{k}')P_{21}(k,z), \qquad (3)$$

with δ^D being a Dirac delta function and $\widetilde{\Delta T}_{21}(\mathbf{k},z)$ denoting the spatial Fourier transform[1] of $\Delta T_{21}(\mathbf{r},z)$, the spatial fluctuations of the 21 cm brightness temperature contrast T_{21} with respect to the CMB. On the right hand side of

Eq. (3), we have written $P_{21}(k,z)$ rather than $P_{21}(\mathbf{k},z)$, under the assumption that the cosmological signal is statistically isotropic. In practice, this assumption enters when estimates of the power spectrum are averaged in bins of constant $k = |\mathbf{k}|$. Note that in principle, the scatter in power within each such bin contains information, since the sample variance is proportional to the power spectrum signal itself. Our expression for the Fisher matrix does not include this information contribution, since it has been shown to be small (Ewall-Wice et al., submitted).

Calculating the derivatives of the power spectrum for Eq. (2) requires a model of reionization. Throughout this paper, we use the publicly available `21cmFAST` package (Mesinger et al. 2011) to simulate reionization, which employs the excursion set formalism of Furlanetto et al. (2004) to compute ionization fields from simulated density fields. The package then uses the density, velocity, and ionization fields to compute the 21 cm brightness temperature contrast against the CMB using (Furlanetto et al. 2006; Loeb & Furlanetto 2013)

$$T_{21}(\hat{\mathbf{n}}, \nu) \approx 27x_{\text{HI}}(1 + \delta_b)\left(1 - \frac{T_{\text{CMB}}}{T_s}\right)\left(\frac{1}{1 + H^{-1}\partial v_r/\partial r}\right)$$
$$\times \left(\frac{1+z}{10}\frac{0.14}{\Omega_m h^2}\right)^{\frac{1}{2}}\left(\frac{\Omega_b h^2}{0.022}\right) \text{mK}, \quad (4)$$

where x_{HI} is the neutral fraction of the hydrogen atoms, T_{21} is the temperature contrast against the CMB, δ_b is the baryon overdensity, T_{CMB} is the CMB temperature, T_s is the spin temperature, Ω_m is the normalized matter density, Ω_b is the normalized baryon density, h is the Hubble parameter (in units of $100\,\text{km/s/Mpc}$), and $\partial v_r/\partial r$ is the derivative of the comoving radial peculiar velocity with respect to the comoving radial distance. During the reionization epoch, the IGM temperature is expected to be coupled to the spin temperature T_s, and is often assumed to have been pre-heated to a high temperature (from, say, early sources of X-rays or structure formation shocks). It is thus common to assume that $T_s \gg T_{\text{CMB}}$ (Zaldarriaga et al. 2004), and with this approximation the spin temperature drops out of Eq. (4). This significantly shortens the computational time of `21cmFAST`, since the evolution of T_S is in general complicated to compute. With this paper focused on the reionization epoch, we make the $T_s \gg T_{\text{CMB}}$ assumption throughout. Once the T_{21} field is obtained, the global signal $\overline{T}_{21}$ can be easily computed by averaging over all sky angles. Subtracting this mean signal from the simulated brightness temperature fields, the power spectrum can then be found using Eq. (3).

To compute the error $\varepsilon(k,z)$ of our power spectrum measurement, we make use of the `21cmSense` code[2] (Parsons et al. 2012a; Pober et al. 2013, 2014). We assume that HERA consists of a tightly packed hexagonal array of 331 dishes, each with a diameter of 14 m. The dishes are non-pointing, and thus all HERA observations will be drift-scan surveys. HERA is optimized for measurements between 100 and 200 MHz, although there are plans to extend the lower end of this range. For the power spectrum forecasts in this paper, we assume 1080 hrs of observations. To account for

---

[1] We adopt a Fourier convention where the forward transform is given by $\tilde{f}(\mathbf{k}) = \int f(\mathbf{r})e^{-i\mathbf{k}\cdot\mathbf{r}}d^3\mathbf{r}$ and the inverse Fourier transform is given by $f(\mathbf{r}) = \int \tilde{f}(\mathbf{k})e^{i\mathbf{k}\cdot\mathbf{r}}\frac{d^3\mathbf{k}}{(2\pi)^3}$.

[2] https://github.com/jpober/21cmSense

foreground contamination, we employ the "moderate foregrounds" setting of `21cmSense`. This setting assumes that foregrounds are spectrally smooth, and thus can be mostly eliminated by filtering out low $k_\parallel$ spatial modes, where $k_\parallel$ is the spatial wavenumber along the line-of-sight (frequency) axis of observations. The threshold value of filtered $k_\parallel$ modes is baseline dependent, with more modes filtered out from data from long baselines. This is because longer baselines tend to be more chromatic, leading to a greater leakage of intrinsically smooth foregrounds to higher $k_\parallel$ modes. For details, please see Datta et al. (2010); Parsons et al. (2012b); Morales et al. (2012); Vedantham et al. (2012); Trott et al. (2012); Thyagarajan et al. (2013); Pober et al. (2014); Liu et al. (2014a,b); Thyagarajan et al. (2015a,b).

In the parameter forecasts that follow, we will explore two fiducial scenarios. The first scenario is based on the best-fit cosmological parameters from *Planck's* TT + lowP dataset. The astrophysical parameters needed to run the reionization simulation are then chosen so that when `21cm-FAST` is run with the best-fit cosmological parameters, the resulting density and ionization fields predict an optical depth τ to the CMB that matches the best-fit τ from the dataset. We follow a similar procedure for *Planck's* TT,TE,EE + lowP + lensing + ext dataset. With these two datasets, we roughly encompass the range of datasets in Planck Collaboration et al. (2015b): TT + lowP has some of the larger parameter errors and one of the highest redshifts of reionization, while TT,TE,EE + lowP + lensing + ext has some of the tightest errors and one of the lowest redshifts of reionization. When analyzing simulated data from the TT+lowP dataset, we assume that the data span $7.5 < z < 13$ and is divided into redshift bins of width $(\Delta z)_{\rm bin} = 0.5$ before power spectra are generated separately for each bin; for the TT,TE,EE + lowP + lensing + ext dataset we assume a range of $6.1 < z < 13$ divided into bins of width $(\Delta z)_{\rm bin} = 0.3$. In determining these specifications, the redshift ranges were mostly arbitrary, with the final results changing negligibly if we simply use the full redshift range of HERA for both datasets. Determining the bin widths is more subtle. Thicker bins mean that larger survey volumes go into the computation of each power spectrum, reducing both cosmic variance and instrumental noise errors. However, thicker bins also mean a more coarse-grained picture of how the power spectrum evolves with redshift, and previous works have shown that redshift evolution is a powerful way to break astrophysical parameter degeneracies (Pober et al. 2014; Greig & Mesinger 2015). There is thus an optimization problem to be solved, but we leave a definitive treatment of this to future work, as it would require a detailed treatment of light-cone effects (Barkana & Loeb 2006; Datta et al. 2012, 2014; Zawada et al. 2014; La Plante et al. 2014), which are neglected in this paper. Our choices of $(\Delta z)_{\rm bin} = 0.3$ and $(\Delta z)_{\rm bin} = 0.5$ were motivated by simple numerical tests that indicated reasonably good performance, and are not to be taken as the results of a rigorous optimization.

2.2 Astrophysical and cosmological parameter constraints

For our parameter estimation forecasts, we pick the parameter set $\boldsymbol{\theta} = [\Omega_b h^2, \Omega_c h^2, \theta_{\rm MC}, \ln(10^{10} A_s), n_s, \tau, T_{\rm vir}, R_{\rm mfp}, \zeta]$, where Ω_c is the normalized cold dark matter density, $\theta_{\rm MC}$

is the approximate angular size of the sound horizon at recombination (as defined by the `CosmoMC` package; Lewis & Bridle 2002), A_s is the amplitude of primordial scalar fluctuations, n_s is the scalar spectral index, $T_{\rm vir}$ is the minimum virial temperature of the first ionizing galaxies, $R_{\rm mfp}$ is the mean free path of ionizing photons in ionized regions, ζ is the ionizing efficiency, and the rest of the parameters are as they were defined above.

Table 1 shows the parameter errors from *Planck* (columns labeled "Errors"; Planck Collaboration et al. 2015b) and the improved errors resulting from adding 21 cm power spectrum measurements from HERA (columns labeled "$+P_{21}(k)$"). All quoted errors correspond to 68% confidence regions after having marginalized over all other parameters.[3] Note that we assume all parameters (whether cosmological or astrophysical) are varied simultaneously; this is in contrast to Pober et al. (2014), which only dealt with the astrophysical parameters and assumed that cosmological parameters were known. We find that such a simultaneous variation of parameters is important even if one is primarily interested in only the astrophysical parameters. This is illustrated in Fig. 1, where pairwise parameter constraints on the three reionization astrophysics parameters, $T_{\rm vir}$, $R_{\rm mfp}$, and ζ are shown. Dark contours delineate 95% confidence regions, while light contours delineate 68% confidence regions. Red contours show the constraints that can be obtained if cosmological parameters are known perfectly, whereas blue contours show the degraded constraints that result from marginalizing over *Planck*-level spreads in the cosmological parameters. The 95% confidence regions of the former are often roughly the same size as the 68% confidence regions of the latter, making it clear that cosmological parameter uncertainties are non-negligible.
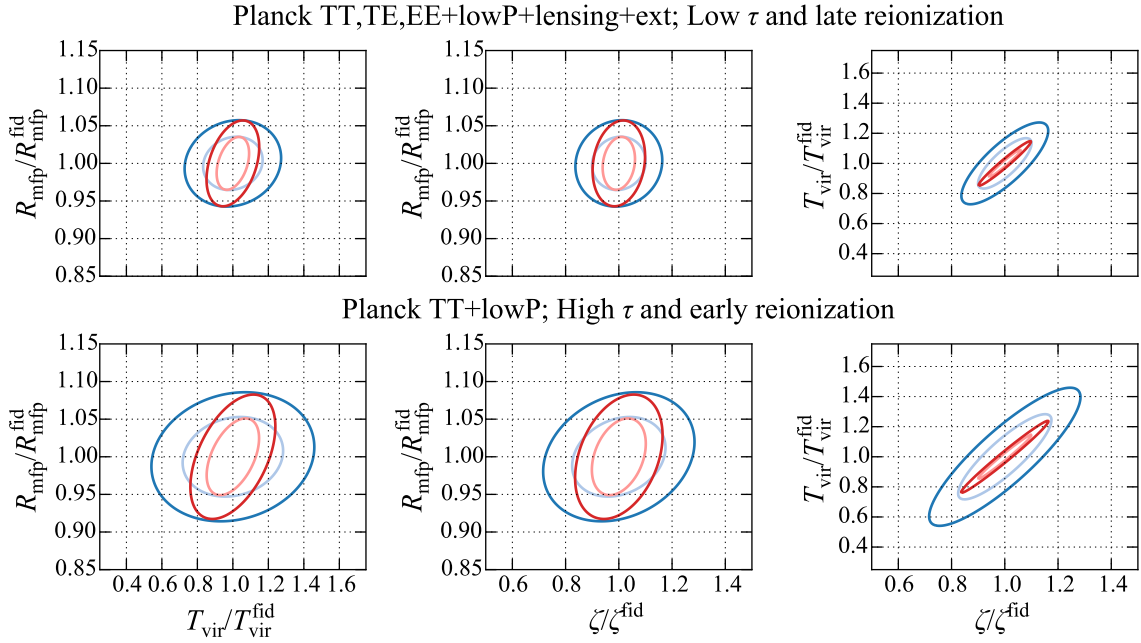
Examining the values in Table 1, one sees that 21 cm power spectrum measurements are more effective at constraining reionization astrophysics if the best-fit parameters have a lower τ value, implying a lower redshift of reionization (as is the case for TT,TE,EE + lowP + lensing + ext compared to TT + lowP). If reionization happens later, characteristic features in the evolution of the 21 cm power spectrum (such as the peak in power at 50% ionization fraction Lidz et al. 2008; Bittner & Loeb 2011) occur at higher frequencies, where both foregrounds and instrumental noise are weaker. This speaks to a natural complementarity between the CMB and 21 cm cosmology when it comes to constraining reionization. For example, if reionization occurs at high redshifts, 21 cm measurements become harder. But τ is then larger, and the "reionization bump" feature of CMB polarization power spectra (Zaldarriaga 1997) becomes easier to measure, reducing the errors on CMB-derived reionization constraints.

For the cosmological parameter constraints, the bene-

---

[3] For reasons of numerical stability, we treat the $\theta_{\rm MC}$ parameter a little differently from the other cosmological parameters. We assume that the 21 cm power spectrum does not directly constrain $\theta_{\rm MC}$. This means that any reductions in the errors on $\theta_{\rm MC}$ come from breaking degeneracies from other parameters, and not from direct measurements. In practice, this has a negligible effect on the results, since $\theta_{\rm MC}$ is determined to such high precision from CMB results alone. We do the same for the global signal constraints on $R_{\rm mfp}$ computed in Sec. 3.

Table 1. Parameter estimation forecasts for astrophysical and cosmological parameters. All quoted errors represent marginalized 68% intervals. The columns labeled "Errors" list the error bars obtained from the *Planck* satellite (Planck Collaboration et al. 2015a,b). The "+$P_{21}(k)$" columns show the effect of adding 21 cm power spectrum data from HERA, while the "+$T_{21}^8(\nu)$" columns additionally include a global signal experiment requiring an eighth order polynomial foreground fit in ln ν. Adding 21 cm power spectrum information to existing constraints results in reduced errors on many cosmological parameters (in addition to producing the first measurements of the astrophysical parameters governing reionization). The further addition of global signal information, however, does little to improve parameter errors. One also sees that the predicted errors are smaller when assuming fiducial values tied to the *Planck* TT,TE,EE+lowP+lensing+ext dataset than when they take their *Planck* TT+lowP values. The "+$P_{21}(k)$" values in this table are reproduced in (Liu et al. 2015), which builds on this paper to explore how a precise understanding of reionization from 21 cm cosmology can improve CMB constraints.

| | | *Planck* **TT + lowP** | | | *Planck* **TT,TE,EE+lowP+lensing+ext** | | | |
	Best fit	Errors	+$P_{21}(k)$	+$T_{21}^8(\nu)$	Best fit	Errors	+$P_{21}(k)$	+$T_{21}^8(\nu)$
Cosmological parameters								
$\Omega_b h^2$	0.02222	±0.00023	±0.00021	±0.00021	0.02230	±0.00014	±0.00013	±0.00013
$\Omega_c h^2$	0.1197	±0.0022	±0.0021	±0.0021	0.1188	±0.0010	±0.00096	±0.00095
$100\theta_{MC}$	1.04085	±0.00046	±0.00046	±0.00045	1.04093	±0.00030	±0.00029	±0.00029
$\ln(10^{10}A_s)$ ...	3.089	±0.036	±0.023	±0.022	3.064	±0.023	±0.016	±0.016
n_s	0.9655	±0.0062	±0.0057	±0.0056	0.9667	±0.0040	±0.0037	±0.0037
τ	0.078	±0.019	±0.013	±0.013	0.066	±0.012	±0.0089	±0.0089
Astrophysical parameters								
T_{vir} [K]	40000	—	±7500	±7400	60000	—	±6700	±6500
R_{mfp} [Mpc] ...	35.0	—	±1.2	±1.2	35.0	—	±0.82	±0.82
ζ	40.0	—	±4.6	±4.5	30.0	—	±2.0	±1.9

Planck TT,TE,EE+lowP+lensing+ext; Low τ and late reionization

Planck TT+lowP; High τ and early reionization

Figure 1. Forecasted astrophysical parameter constraints from HERA. Light contours signify 68% confidence regions, while dark contours denote 95% confidence regions. Axes are scaled according to fiducial values chosen to match *Planck's* TT,TE,EE+lowP+lensing+ext data (top row) and *Planck's* TT+lowP data (bottom row). Red contours assume that cosmological parameters are known, whereas blue contours marginalize over cosmological parameter uncertainties. Though the CMB (in conjunction with other cosmological probes) has delivered exquisite constraints on cosmological parameters, we see that the residual uncertainties still have a non-negligible effect on astrophysical parameters derived from 21 cm power spectrum measurements. When only astrophysical parameters are varied (red contours), the constraints are in rough agreement with those found in Pober et al. (2014), although direct comparisons should be interpreted with caution given the different priors on fiducial parameters.

fits from adding 21 cm power spectrum measurement clearly vary from parameter to parameter. For example, errors in $\Omega_b h^2$, $\Omega_c h^2$, and θ_{MC} are essentially unchanged, while A_s, n_s, and τ do show some improvement. Within the semi-analytic simulations of `21cmFAST`, A_s has a reasonably strong effect on the 21 cm power spectrum, since a higher A_s means that density peaks will more quickly reach the threshold densities necessary to ionize, pushing reionization to higher redshifts. A change in n_s can similarly change the amount of structure formation on scales relevant to ionizing galaxies, since such scales are quite different from the pivot scale of a power-law primordial matter power spectrum. Reasoning backwards, it is thus unsurprising that a measurement of the 21 cm power spectrum provides additional constraints on these parameters and reduce their errors.

In contrast, the improvement in errors on τ arises for different reasons. In simulations of reionization, τ is typically not an independent parameter that can be varied; rather, it is a *prediction* that can be extracted from the simulated density and ionization fields, given the other model parameters. Imposing self-consistency between this prediction and the best-fit τ value derived from CMB data can then provide an additional opportunity to improve constraints on both τ and the other parameters. In this paper, we do not impose this self-consistency condition, leaving a discussion of its impact to Liu et al. (2015). With our current treatment, τ errors are reduced with the addition of 21 cm only because A_s and τ obey a tight degeneracy when constrained from CMB data alone (with $A_s e^{-2\tau}$ measured with much higher precision than either A_s or τ alone). Reducing A_s errors thus reduces τ errors.
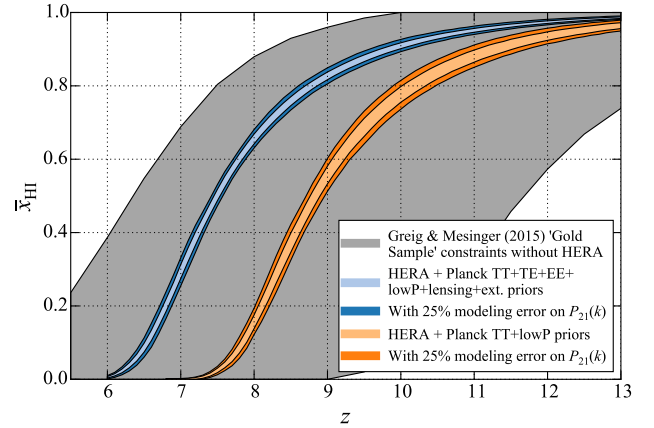
2.3 Ionization history constraints

The parameter constraints derived in the previous section can be translated into errors on the angle-averaged ionization history by drawing random realizations of parameters consistent with our predicted parameter covariances, and then running a simulation of the ionization field for each realized parameter set. The spread in the resulting ionization histories provides an estimate of the error in the ionization history from a power spectrum-based constraint.

In practice, even fast semi-analytic codes such as `21cmFAST` are insufficiently quick to allow this procedure to followed if cosmological parameters are varied along with the astrophysical parameters. Assuming that errors about fiducial parameters are small, we instead adopt a linearized approach. Denoting by Δp the shift in the parameter p from its fiducial value, the angle-averaged neutral fraction $\overline{x}_{\mathrm{HI}}$ is given by

$$\overline{x}_{\mathrm{HI}}(z) = \overline{x}_{\mathrm{HI}}^{\mathrm{fid}}(z) + \sum_{\gamma} h_{\gamma}(z)\Delta p_{\gamma}, \qquad (5)$$

where $x_{\mathrm{HI}}^{\mathrm{fid}}$ is the fiducial ionization history corresponding to the fiducial parameters (i.e. with $\Delta p_{\gamma} = 0$), and $h_{\gamma}(z)$ is the redshift-dependent response of the ionization history to a shift in the γth parameter (which we compute using training runs of `21cmFAST`).

Fig. 2 shows the resulting ionization history constraints from HERA. In light orange is the 95% confidence region assuming *Planck* TT + lowP fiducial parameters, while the 95% confidence region assuming *Planck* TT,TE,EE + lowP

Figure 2. Forecasts for constraints on the neutral fraction history $\overline{x}_{\mathrm{HI}}(z)$ from HERA power spectrum measurements. A neutral fraction (or equivalently, ionization) history can be obtained from power spectrum measurements by first fitting the power spectra to predictions from semi-analytic reionization codes like `21cmFAST`, in the process obtaining best-fit values for the astrophysical and cosmological parameters listed in Table 1. These parameters can then be fed back into the code to prediction the ionization history. The light blue band shows the expected 95% confidence region for the neutral fraction history predicted from such a procedure, tuned to fit the fiducial parameters from *Planck's* TT,TE,EE+lowP+lensing+ext dataset. The dark blue band shows the corresponding region if the semi-analytic codes are assumed to have a 25% modeling error in their prediction of the 21 cm power spectrum. Analogous constraints assuming fiducial values from *Planck's* TT+lowP dataset are shown in orange. These forecasts compare favorably to the combined "gold sample" constraints (grey band) from Greig & Mesinger (in prep.).

+ lensing + ext fiducial parameters is shown in light blue. In both cases, we simultaneously account for uncertainties in astrophysical and cosmological parameters, i.e., the confidence regions reflect uncertainties in all the parameters listed in Table 1 except τ, which is not needed in the reionization simulations. Again, we see that the projected constraints are tighter if reionization happens later, but in either scenario HERA is able to make a precise measurement. Of course, this measurement is necessarily model-dependent, since the 21 cm power spectrum measurement does not directly measure the ionization history. To account for the model dependence, the dark blue and dark orange band show the results from incorporating a modeling error in the power spectrum constraints. We follow the treatment in Greig & Mesinger (2015) and crudely add an uncorrelated modeling error to each k bin at a level of 25% of the fiducial power spectrum, in quadrature with the errors computed by `21cmSense`. This essentially incorporates a bin-by-bin amplitude error in our modeling of the power spectrum. The increased errors then result in greater astrophysical and cosmological parameter uncertainties, which translate into greater uncertainties in the ionization history. One sees that the final constraints remain tight. In addition to the amplitude errors, there also exists a generous allowance for possible modeling errors in the *timing* of reionization, with our ionization history constraints remaining relevant even if broadened by,

say, $\Delta z \sim 0.5$ or 1. This can be seen by comparing the HERA constraints to the grey band in Fig. 2, which is reproduced from the combined "gold sample" constraints of Greig & Mesinger (in prep.). To obtain these constraints, Greig & Mesinger used `21cmFAST` simulations within a Bayesian framework to combine constraints from the *Planck* optical depth with those from dark pixels in the Lyα and Lyβ forests (McGreer et al. 2015). The 21 cm line is seen to have much to contribute.

3 COMBINING POWER SPECTRUM AND GLOBAL SIGNAL MEASUREMENTS VIA JOINT FITS

Having provided updated power spectrum parameter constraints, we now consider how global signal and power spectrum measurements can complement one another. In this section, we examine what is arguably the simplest way to combine two complementary datasets—a joint fit for the same model parameters with both datasets.

Global signal measurements measure the 21 cm brightness temperature averaged over the entire sky. In other words, global signal experiments do not resolve the spatial variations of the brightness temperature field. The goal is instead to average over these variations to obtain an average brightness temperature $\overline{T}_{21}$ as a function of redshift (or equivalently, frequency). Typically, the global signal is accessed by a single antenna with a spatial response that is broad enough to essentially perform the requisite average over the sky. As our worked example, we assume that this antenna is pointed towards the Northern Galactic Pole (NGP), with a beam pattern $A(\theta, \varphi)$ given by

$$A(\theta, \varphi) = \exp\left(-\frac{1}{2}\frac{\theta^2}{\theta_b^2}\right)\cos\theta, \qquad (6)$$

where θ is the polar angle from the NGP, φ is the azimuthal angle, and we take θ_b to be 0.3 rad at 120 MHz. We assume a frequency range of 120 MHz to 200 MHz. To account for foreground contamination, a common approach is to fit the measured spectra with low order polynomials. The expectation is that foregrounds are typically spectrally smooth, and can therefore be accounted for by low-order fits. In this section, we use Legendre polynomials as an orthogonal basis for our fits. Explicitly, the foreground contribution $\overline{T}_{\mathrm{fg}}(\nu)$ to the global signal is modeled as

$$\overline{T}_{\mathrm{fg}}(\nu) = \exp\left[\sum_{i=0}^{N_p} a_i p_i\left(\frac{\ln \nu - \ln \nu_0}{\Delta_{\ln \nu}}\right)\right], \qquad (7)$$

where p_i is the ith Legendre polynomial, $\{a_i\}$ are the foreground model parameters to be fit for in the data, and N_p is the order of foreground polynomial. The quantities ν_0 and $\Delta_{\ln \nu}$ are defined for convenience so that if $\nu_{\min}$ and $\nu_{\max}$ are the minimum and maximum observation frequency, respectively, we have $\ln \nu_0 \equiv (\ln \nu_{\min} + \ln \nu_{\max})/2$ and $\Delta_{\ln \nu} \equiv (\ln \nu_{\max} - \ln \nu_{\min})/2$. Following Bernardi et al. (2015), we assume that eighth order polynomials are sufficient to fit out the foregrounds, although in Sec. 4 we varying N_p to examine the impact that foregrounds may have on a detection of the global signal.

To forecast the performance of a global signal experiment, we again employ the Fisher matrix formalism. The

Fisher matrix is given by (Pritchard & Loeb 2010; Bernardi et al. 2015; Presley et al. 2015)

$$\mathbf{F}^{\mathrm{GS,FG}}_{\alpha\beta} = \sum_i \frac{1}{\varepsilon^2_{\mathrm{GS}}(\nu_i)} \frac{\partial \overline{T}_{\mathrm{tot}}(\nu_i)}{\partial \phi_\alpha} \frac{\partial \overline{T}_{\mathrm{tot}}(\nu_i)}{\partial \phi_\beta}, \qquad (8)$$

where $\overline{T}_{\mathrm{tot}} \equiv \overline{T}_{\mathrm{fg}} + \overline{T}_{21}$ is the total (foregrounds plus cosmological) signal measured by an instrument, and ϕ_α is the αth parameter in the set of model parameters $\boldsymbol{\phi}$, which consists of $\boldsymbol{\theta}$ plus the polynomial coefficients used to fit for foregrounds. The instrumental noise error in the measurement of $\overline{T}_{\mathrm{tot}}$ is denoted by $\varepsilon_{\mathrm{GS}}$. To combine the Fisher information from the global signal with that from power spectrum, we must first marginalize over the nuisance foreground coefficients. Operationally, this means inverting $\mathbf{F}^{\mathrm{GS,FG}}$ to obtain a covariance matrix for the parameter set $\boldsymbol{\phi}$, deleting the rows and columns corresponding to the foreground coefficients, and inverting once more to obtain a smaller Fisher matrix $\mathbf{F}^{\mathrm{GS}}$ for the parameter set $\boldsymbol{\theta}$. The final Fisher matrix for a joint fit between results from a power spectrum and a global signal measurement is then obtained by summing $\mathbf{F}^{\mathrm{PS}}$ and $\mathbf{F}^{\mathrm{GS}}$.

The parameter forecasts for a combined fit are shown in the "$+T_{21}^8(\nu)$" column of Table 1. One sees that a global signal experiment targeting the reionization epoch (i.e., covering frequency ranges above $\sim 100\,\mathrm{MHz}$) adds little to parameter constraints (whether astrophysical or cosmological) already provided by the power spectrum measurements. This is consistent with the results found in Mirocha et al. (2015), which highlighted the importance of broadband measurements that reach the high redshifts of the prereionization era. During reionization, the global signal is essentially smooth and featureless, and takes the simple form of a slow decay to zero brightness temperature as the neutral hydrogen fraction approaches zero (see, for instance, the solid black curves in Fig. 4). With so few features to constrain, observations of the global signal during reionization are highly degenerate in their determination of model parameters, particularly when nuisance parameters from the spectrally smooth foregrounds are included. Instead of seeking constraints on physical model parameters, global signal measurements from reionization are far better suited for capturing broad phenomenological parameters such as the rough redshift and duration of reionization.

4 USING A POWER SPECTRUM MEASUREMENT TO AID A GLOBAL SIGNAL MEASUREMENT

In the previous section, we saw that joint fits of data from power spectrum and global signal experiments are unlikely to reduce errors in astrophysical and cosmological parameter constraints, at least if measurements are limited to the reionization epoch. Furthermore, joint fits implicitly assume a correct underlying model that can accurately predict the behavior of all the datasets involved. In this section, we take a step back and explore a model-influenced but largely model-independent method for using power spectrum results to enhance a global signal measurement.

Unlike power spectrum measurements, which must deal with the dual challenges of sensitivity and foreground contamination, global signal measurements are typically not

lacking in sensitivity (Presley et al. 2015). The necessary signal-to-noise can be achieved after ~ 100 hours of high quality observations with a single dipole, whereas power spectrum measurements require roughly an order of magnitude more integration time even with the largest low-frequency arrays in existence. The chief obstacle to a successful measurement of the global signal is then foreground contamination.

Foregrounds are more difficult to deal with in global signal experiments than they are for power spectrum measurements. This is simply because fewer numbers are measured. In particular, if the global signal spectrum is measured at $N_{\rm chan}$ different spectral channels, it is mathematically impossible to simultaneously constrain the $2N_{\rm chan}$ degrees of freedom from $N_{\rm chan}$ channels of the cosmological signal and the $N_{\rm chan}$ channels of the foreground signal. One way to deal with this problem is to increase the number of measurements. For example, angular information can be recorded, increasing the number of independent measurements to $N_{\rm chan}N_{\rm pix}$, where $N_{\rm pix}$ is the number of independent pixels surveyed on the sky. This extra information can then be used to aid foreground subtraction (Liu et al. 2013). Alternatively, if the number of measurements is held fixed at $N_{\rm chan}$, one can decrease the number of parameters that one is trying to constrain. In one extreme, for example, if the foreground spectrum is known perfectly, it can simply be subtracted directly from the measured spectrum, leaving only the cosmological contribution to the signal at $N_{\rm chan}$ different frequencies. More realistically, the foregrounds are not known perfectly, and assumptions need to be made regarding the possible forms of the foreground and cosmological signal contributions. In practice, these assumptions are often encapsulated by the specific parametric forms that are chosen to fit the data.

The success of a global signal experiment thus depends on our ability to compactly describe the foregrounds and the cosmological signal in as few parameters as possible (Switzer & Liu 2014). The parameterization of foreground spectra has already been considered elsewhere in the literature, with most treatments fitting out foregrounds using smooth functions like low-order polynomials. As with the previous section, we will continue to parameterize the foregrounds as a series of low-order orthogonal Legendre polynomials in $\ln \nu$. Our goal is instead to tackle the problem of how one might parameterize the cosmological signal. Two popular parameterizations of the global signal—the turning point model and the tanh model—have been recently compared in Harker et al. (2015). Here we propose a third.

Suppose one has made a successful detection of the 21 cm power spectrum. Further suppose that using this data (possibly along with other datasets), one has inferred a set of best-fit values for a set of astrophysical and cosmological parameters (such as those shown in Table 1). These best-fit values can then be used to predict a fiducial global signal $T_{21}^{\rm fid}(\nu)$ by running reionization simulations such as `21cmFAST`. This fiducial global signal can then be treated as first guess of the true global signal, and a global signal measurement can be used to measure *deviations* from this fiducial signal. Note that in redefining the goals of a global signal measurement in this way, we have not formally improved our situation. The fiducial global signal acts only as a frequency-dependent offset in our measurement, and does
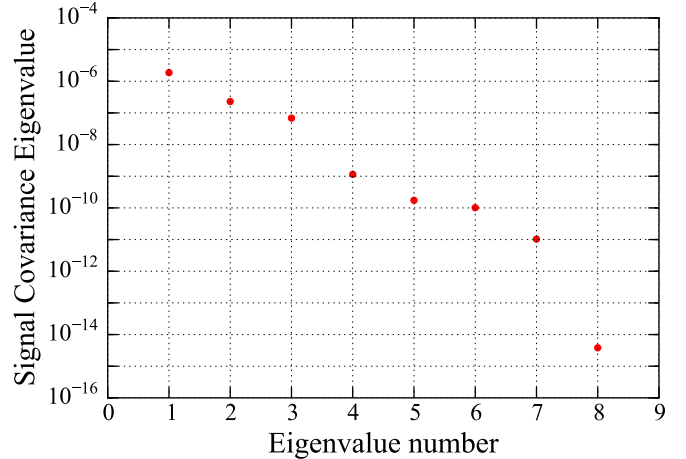
Figure 3. The first few eigenvalues of **S** (Eqs. 10 and 11), assuming a covariance matrix **C** of astrophysical and cosmological parameters from HERA. The exponential fall-off seen in this plot suggests that once the relevant astrophysical and cosmological parameters have been measured to reasonable precision by a power spectrum experiment, the allowable deviations of the global signal from a fiducial model (encoded by **S**) can be captured by a small number of parameters.

not reduce the number of degrees that one must fit for. To do so, we must identify the ways in which the global signal is likely to deviate, given the uncertainties in our modeling of reionization that still remain after the power spectrum measurement. This can be done using a similar approach to the one that we adopted for the ionization history in Sec. 2.3. We approximate the global signal as

$$\overline{T}_{21}(\nu) \approx \overline{T}_{21}^{\rm fid}(\nu) + \sum_\gamma g_\gamma(\nu)\Delta p_\gamma, \tag{9}$$

where $g_\gamma(\nu)$ is the response of the global signal to a shift in the γth parameter from its fiducial (or best-fit) value, and Δp_γ is again the size of this shift. The statistically likely deviations in the global signal can then be captured by a signal covariance matrix

$$\mathbf{S}_{ij} \equiv \langle \overline{T}_{21}(\nu_i)\overline{T}_{21}(\nu_j)\rangle - \overline{T}_{21}^{\rm fid}(\nu_i)\overline{T}_{21}^{\rm fid}(\nu_j), \tag{10}$$

where in this equation (unlike with Eq. 1) the angled brackets $\langle \ldots \rangle$ signify an ensemble average over variations in the parameters, and thus $\langle \overline{T}_{21}(\nu)\rangle = \overline{T}_{21}^{\rm fid}(\nu)$ by definition. Inserting Eq. (9) into the definition of **S** then gives

$$\mathbf{S} = \mathbf{G}\mathbf{C}\mathbf{G}^t, \tag{11}$$

where $\mathbf{G}_{i\alpha} \equiv g_\alpha(\nu_i)$ and **C** is the covariance matrix of the parameters. In other words, interpreting the parameter deviations in Eq. (9) as being due to uncertainties in the best-fit parameters from the power spectrum measurement, we have $\mathbf{C}_{\alpha\beta} \equiv \langle \Delta p_\alpha \Delta p_\beta \rangle$.

To identify the spectral modes that represent the likeliest deviations from the fiducial global signal, we perform an eigenvalue decomposition of **S**. If the eigenvalues are dominated by a handful of large values, then plausible forms for the global signal (in the context of the limitations imposed by the measured astrophysical and cosmological parameters and the physical constraints of reionization simulations) can
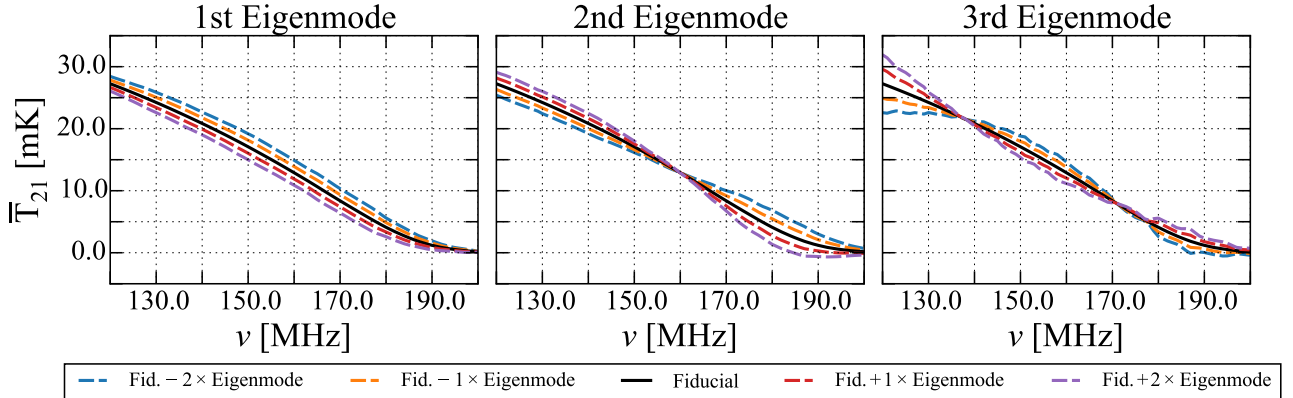
Figure 4. Fiducial global signal (solid black) perturbed by the first deviation eigenmode (left plot), second eigenmode (center plot), and the third eigenmode (right plot). In each plot, both positive and negative perturbations to the fiducial model are shown. The first eigenmode is seen to mostly shift the redshift of the midpoint of reionization without altering its duration, while the second eigenmode changes the duration while keeping the midpoint constant. Higher eigenmodes add increasingly complicated features to the global signal.

be captured by just a small number of eigenmodes. We see precisely this behavior in Fig. 3, where the eigenvalues of **S** are seen to fall off exponentially. Intuition for the first few eigenmodes can be obtained by examining Fig. 4, where we show examples of how each eigenmode perturbs the fiducial global signal. The first eigenmode is seen to mostly control the redshift of the midpoint of reionization without affecting its duration. The second eigenmode affects the duration without affecting the midpoint. The third eigenmode accounts for higher order curvature effects in the global signal history. Taken together, these results suggest that even though the details of reionization depend on astrophysical and cosmological parameters in complicated ways, uncertainties in these model parameters can only induce rather specific types of changes in the global signal. Thus, an economical model (in the sense of having few parameters) for the cosmological global signal is given by

$$\overline{T}_{21}(\nu) \approx \overline{T}_{21}^{\rm fid}(\nu) + \sum_i^{N_d} b_i d_i(\nu), \qquad (12)$$

where $d_i(\nu)$ is the ith eigenmode of **S**, and it is assumed that N_d such "deviation eigenmodes" are sufficient to capture deviations from the fiducial model in the measurement. The coefficients $\{b_i\}$ are the parameters to be fit in an analysis of global signal data. Once these are determined, they can reinserted into Eq. (12) for an estimate of the global signal.

Under our proposed data analysis scheme, the forecasted performance of a global signal measurement will be somewhat tied to the performance of a power spectrum experiment. This is because our parameterization of the cosmological global signal requires prior information from a power spectrum measurement, entering via Eq. (11) as the covariance matrix **C** of astrophysical and cosmological parameters. As our worked example, we will again use HERA, obtaining **C** from the Fisher forecasts of Sec. 2.2 for the *Planck* TT,TE,EE+lowP+lensing+ext scenario (the results for *Planck* TT+lowP being qualitatively similar). Importantly, however, our global signal forecasts do not depend on the *amplitude* of the parameter errors from the power
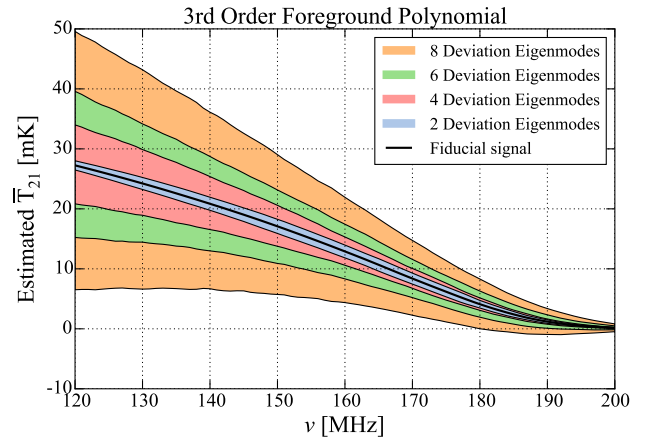
Figure 5. Forecasted global signal recovery, assuming that foregrounds can be adequately described by a third order (i.e., cubic) polynomial in $\ln \nu$. The quality of the recovery depends on the number of deviation eigenmodes that are needed to obtain a good fit to the cosmological global signal. Each colored band shows the 95% confidence region of the recovered signal for a different number of deviation eigenmodes.

spectrum measurements, only the *shapes* of parameter degeneracies. To see this, notice that rescaling **C** by an overall constant results only in a corresponding rescaling of **S**, which affects its eigenvalues but not its eigenvectors (i.e., the deviation eigenmodes). Such a rescaling therefore has no effect on the parameterization given by Eq. (12), and once the deviation eigenmodes $\{d_i(\nu)\}$ are determined we no longer require knowledge of our power spectrum experiment.

With deviation eigenmodes in hand, we may push forward to a global signal forecast, again employing the Fisher matrix formalism. The procedure is essentially the same as the one employed in the previous section, except with the expansion coefficients of Eq. (12) taking the place of the astrophysical and cosmological parameters. The foreground-
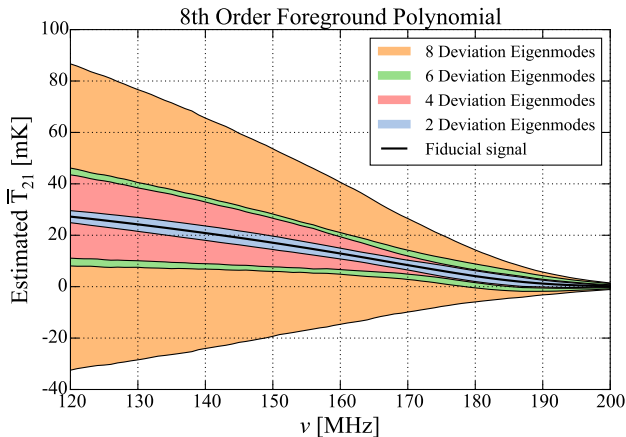
Figure 6. Same as Fig. 5 but assuming that a successful foreground fit requires an eighth order polynomial in $\ln \nu$. Compared to Fig. 5, the recovery of the global signal is clearly degraded. However, reasonably precise constraints can still be obtained if deviations from the fiducial model can be adequately described by a small number of deviation eigenmodes.

marginalized Fisher forecasts are then used to draw random realizations of $\{b_i\}$, which are in turn propagated into confidence regions for $\overline{T}_{21}(\nu)$ using Eq. (12). The results are shown in Figs. 5 and 6, assuming that foregrounds can be adequately fit using polynomials of order three and eight, respectively. The former is intended to represent the relatively optimistic assumption of an instrument with a largely achromatic beam response that does not imprint extra spectral structure onto the smooth foregrounds (Pritchard & Loeb 2010; Morandi & Barkana 2012), while the latter is intended to be reflective of a more pessimistic assumption where chromatic beams or other effects degrade the smoothness of the observed foregrounds (Vedantham et al. 2014; Bernardi et al. 2015; Presley et al. 2015). In each plot, we show the 95% confidence regions of the recovered global signal, with the different colors corresponding to different assumptions regarding the number of eigenmodes that are needed to adequately fit any deviations from the fiducial spectrum.

From these plots, it is clear that the global signal can be measured with high precision if very few deviation eigenmodes are needed to fit the data. For example, we see that if only two modes are necessary, either foreground scenario will yield tight constraints on the global signal. This is perhaps unsurprising, since we saw from Fig. 4 that the first two modes mostly encode information about the timing of reionization, which previous studies have suggested can be inferred reasonably well from global signal experiments (Pritchard & Loeb 2010; Morandi & Barkana 2012; Liu et al. 2013; Presley et al. 2015). As the number of necessary deviation eigenmodes increases, however, a comparison of Figs. 5 and 6 reveals that it is crucial that foreground contaminants be describable by a small number of smooth components.

In this section, we have shown how 21 cm power spectrum measurements can be used to construct a parameterization for the cosmological global signal. The resulting parameterization is designed to economically describe likely deviations from a fiducial global signal using only a small

number of parameters, thus increasing the likelihood of a detection of the global signal amidst foreground contaminants. Importantly, we note that while the parameterization is certainly influenced by the power spectrum measurements and the theoretical models used to interpret them, our scheme is formally model-independent. This is because the eigenmodes of $\mathbf{S}$ form a basis that spans the space of all possible spectra.[4] As a result, even arbitrary deviations from the fiducial model can in principle be captured in our analysis, simply by increasing the number of deviation eigenmodes that one fits for. Our method is thus model-independent, although in practice the precision of the recovered global signal will degrade with the number of modes. Ideally, one should therefore use as few components as are necessary, using model-selection algorithms to select the optimal number of deviation eigenmodes that are demanded by the data, analogous to the way in which Harker (2015) selected the number of foreground components. By using power spectrum results to inform our parameterization, we increase the likelihood of being able to use a small number of components while preserving formal model independence.

Although we saw in Sec. 3 that global signal measurements may not inform parameter constraints, they are still valuable in providing a cross-check on the results of a power spectrum measurement. The most fruitful way to enact such a cross-check will be to check for consistency in the timing of reionization, since Fig. 4 shows that global signal measurements will be particularly sensitive to timing. Moreover, Liu et al. (2015) recently showed that as a direct measurement of the brightness temperature field, the global signal can provide a more model-independent way to remove reionization as a nuisance effect in CMB studies. Finally, our treatment of the global signal in this paper pertains only to those experiments targeting the reionization epoch exclusively. At higher redshifts the global signal takes a more complicated form, and experiments will be able to place precise constraints on the astrophysics of the IGM (Harker et al. 2012; Mirocha et al. 2013, 2015).

5   CONCLUSIONS

In this paper, we have addressed a number of outstanding issues in forecasts for upcoming 21 cm power spectrum and global signal measurements. First, we provided updated forecasts for 21 cm power spectrum measurements seeking to constrain astrophysical and cosmological parameters. Our forecasts are based on two sets of fiducial parameters from the *Planck* satellite. One set is based on the *Planck's* TT+lowP dataset and features a relatively high optical depth τ, while the other is based on *Planck's* TT,TE,EE+lowP+lensing+ext dataset and features a relatively low τ. Using a Fisher matrix formalism, we find that the projected parameter constraints from a power spectrum measurement are better

---

[4] Note that this is true even though $\mathbf{S}$ is in general not a full-rank matrix, and will typically have the same number of non-zero eigenvalues as $\mathbf{C}$. Even without a full set of non-zero eigenvalues, the eigenvectors of $\mathbf{S}$ span the space. To see this, recall that adding the identity matrix to a rank-deficient $\mathbf{S}$ has no effect on its eigenvectors, but will make all the eigenvalues non-zero.

for the TT,TE,EE+lowP+lensing+ext dataset than the TT+lowP dataset. The lower τ of the latter dataset implies a lower redshift of reionization, which is favorable to 21 cm experiments. This is because lower redshifts translate into higher frequencies for 21 cm observations, where the foregrounds are dimmer and instrumental noise is lower. Additionally, the cosmological constraints from the TT,TE,EE+lowP+lensing+ext dataset alone (i.e., without 21 cm information) are tighter than those from TT+lowP. This also contributes to better parameter constraints because instruments like HERA are sensitive enough to make cosmological parameter uncertainties non-negligible in one's data analysis.

Turning to angle-averaged quantities, we have provided the first forecasts of HERA's ability to constrain the ionization history. These forecasts compare favorably to those provided by non-21 cm probes, significantly narrowing the set of plausible histories even if low levels of modeling errors are present in semi-analytic simulations. We also show forecasts of astrophysical and cosmological parameter constraints from joint fits over both power spectrum and global signal measurements. Unfortunately, we find that a global signal measurement limited to the likely redshift range of reionization (say, between $z \sim 6$ and 11) will not add much to the model constraints already provided by power spectrum measurements. This is because the global signal is relatively featureless during reionization, making parameter variations difficult to pick out from shifts in foreground parameters. As suggested in Mirocha et al. (2015), direct constraints on model parameters from global signal experiments will likely require broadband instruments that reach beyond reionization to higher redshifts.

Importantly, however, we note that it is still important to have global signal experiments that target reionization, because our description of the 21 cm brightness temperature field will be incomplete without them. Unlike the CMB, whose sky-averaged signal follows a simple blackbody spectrum at leading order, the mean 21 cm signal (i.e., the global signal) has a non-trivial frequency dependence due to heating and ionization processes in the IGM. A complete description of the 21 cm brightness thus requires not only a quantification of the spatial fluctuations (via the power spectrum, for example), but also the global signal. The global signal additionally provides a good cross-check on power spectrum results, and can enhance CMB constraints in a more model-independent way (Liu et al. 2015). In this paper, we have proposed a method by which the results from a power spectrum measurement can be used to aid a detection of the global signal. Power spectrum measurements are used to measure the underlying parameters of reionization simulations. The reionization simulations are then used to predict plausible global signal histories, with the covariance of the measured parameters translating into a covariance of global signal histories. An eigenvalue decomposition of the latter covariance then provides a basis of "deviation" eigenmodes whose amplitudes can be constrained by global signal experiments. Typically, only a small number of these eigenmodes will represent deviations from fiducial global signal histories that are consistent with both the physical constraints imposed by the simulations and the power spectrum measurements. Thus, if deviations from fiducial models are relatively small, only a few modes will be necessary to fit the global

signal data, enabling a high signal-to-noise measurement. On the other hand, if deviations are large, more modes will be required and the measurement will be degraded. However, because the deviation eigenmodes collectively span the space of all possible global signal histories, our scheme will still allow accurate (if not precise) measurements of the global signal. In other words, while our eigenmode parameterization of the global signal is model-*influenced*, it is not formally model-*dependent*.

This paper reaffirms the promise of 21 cm cosmology, showing that even when cosmological parameter uncertainties are included in one's forecasts, the resulting constraints on astrophysical parameters from power spectrum measurements are still excellent. Moreover, these constraints can then be used to train a spectral basis set for fitting global signal data, boosting the potential for global signal experiments to provide an independent window into the high redshift universe. With improved instruments like HERA being constructed, our forecasts confirm that 21 cm cosmology has the potential to significantly improve our understanding of astrophysics and cosmology.

REFERENCES

Ali Z. S., et al., 2015, ApJ, 809, 61
Barger V., Gao Y., Mao Y., Marfatia D., 2009, Physics Letters B, 673, 173
Barkana R., Loeb A., 2006, MNRAS, 372, L43
Bernardi G., McQuinn M., Greenhill L. J., 2015, ApJ, 799, 90
Bittner J. M., Loeb A., 2011, J. Cosmology Astropart. Phys., 4, 38
Bowman J. D., Rogers A. E. E., 2010, Nature, 468, 796
Bowman J. D., Rogers A. E. E., Hewitt J. N., 2008, ApJ, 676, 1
Bowman J. D., et al., 2013, Publ. Astron. Soc. Australia, 30, 31
Burns J. O., et al., 2012, Advances in Space Research, 49, 433
Christian P., Loeb A., 2013, J. Cosmology Astropart. Phys., 9, 14
Clesse S., Lopez-Honorez L., Ringeval C., Tashiro H., Tytgat M. H. G., 2012, Phys. Rev. D, 86, 123506
Cooray A., Li C., Melchiorri A., 2008, Phys. Rev. D, 77, 103506
Datta A., Bowman J. D., Carilli C. L., 2010, ApJ, 724, 526
Datta K. K., Mellema G., Mao Y., Iliev I. T., Shapiro P. R., Ahn K., 2012, MNRAS, 424, 1877
Datta K. K., Jensen H., Majumdar S., Mellema G., Iliev I. T., Mao Y., Shapiro P. R., Ahn K., 2014, MNRAS, 442, 1491

Dillon J. S., et al., 2014, Phys. Rev. D, 89, 023002
Dillon J. S., et al., 2015, Phys. Rev. D, 91, 123011
Evoli C., Mesinger A., Ferrara A., 2014, J. Cosmology Astropart. Phys., 11, 24
Furlanetto S. R., Zaldarriaga M., Hernquist L., 2004, ApJ, 613, 1
Furlanetto S. R., Oh S. P., Briggs F. H., 2006, Phys. Rep., 433, 181
Gnedin N. Y., Shaver P. A., 2004, ApJ, 608, 611
Greenhill L. J., Bernardi G., 2012, preprint, (arXiv:1201.1700)
Greig B., Mesinger A., 2015, MNRAS, 449, 4246
Greig B., Mesinger A., Pober J. C., 2015, preprint, (arXiv:1509.02158)
Harker G. J. A., 2015, MNRAS, 449, L21
Harker G. J. A., Pritchard J. R., Burns J. O., Bowman J. D., 2012, MNRAS, 419, 1070
Harker G. J. A., Mirocha J., Burns J. O., Pritchard J. R., 2015, preprint, (arXiv:1510.00271)
Hinshaw G., et al., 2013, ApJS, 208, 19
Jacobs D. C., et al., 2015, ApJ, 801, 51
La Plante P., Battaglia N., Natarajan A., Peterson J. B., Trac H., Cen R., Loeb A., 2014, ApJ, 789, 31
Lewis A., Bridle S., 2002, Phys. Rev. D, 66, 103511
Lidz A., Zahn O., McQuinn M., Zaldarriaga M., Hernquist L., 2008, ApJ, 680, 962
Liu A., Pritchard J. R., Tegmark M., Loeb A., 2013, Phys. Rev. D, 87, 043002
Liu A., Parsons A. R., Trott C. M., 2014a, Phys. Rev. D, 90, 023018
Liu A., Parsons A. R., Trott C. M., 2014b, Phys. Rev. D, 90, 023019
Liu A., Pritchard J. R., Allison R., Parsons A. R., Seljak U., Sherwin B. D., 2015, preprint, (arXiv:1509.08463)
Loeb A., Furlanetto S. R., 2013, The First Galaxies In The Universe. Princeton University Press, Princeton, NJ
Mahesh N., Subrahmanyan R., Udaya Shankar N., Raghunathan A., 2014, preprint, (arXiv:1406.2585)
Mao Y., Tegmark M., McQuinn M., Zaldarriaga M., Zahn O., 2008, Phys. Rev. D, 78, 023529
Masui K. W., et al., 2013, ApJ, 763, L20
McGreer I. D., Mesinger A., D'Odorico V., 2015, MNRAS, 447, 499
McQuinn M., Zahn O., Zaldarriaga M., Hernquist L., Furlanetto S. R., 2006, ApJ, 653, 815
Mellema G., et al., 2013, Experimental Astronomy, 36, 235
Mesinger A., Furlanetto S., Cen R., 2011, MNRAS, 411, 955
Mesinger A., Ewall-Wice A., Hewitt J., 2014, MNRAS, 439, 3262
Mirocha J., Harker G. J. A., Burns J. O., 2013, ApJ, 777, 118
Mirocha J., Harker G. J. A., Burns J. O., 2015, preprint, (arXiv:1509.07868)
Morales M. F., Wyithe J. S. B., 2010, ARA&A, 48, 127
Morales M. F., Hazelton B., Sullivan I., Beardsley A., 2012, ApJ, 752, 137
Morandi A., Barkana R., 2012, MNRAS, 424, 2551
Mozdzen T. J., Bowman J. D., Monsalve R. A., Rogers A. E. E., 2015, preprint, (arXiv:1510.03477)
Paciga G., et al., 2013, MNRAS,
Parsons A. R., et al., 2010, AJ, 139, 1468
Parsons A., Pober J., McQuinn M., Jacobs D., Aguirre J., 2012a, ApJ, 753, 81
Parsons A. R., Pober J. C., Aguirre J. E., Carilli C. L., Jacobs D. C., Moore D. F., 2012b, ApJ, 756, 165
Parsons A. R., et al., 2014, ApJ, 788, 106
Patra N., Subrahmanyan R., Raghunathan A., Udaya Shankar N., 2013, Experimental Astronomy, 36, 319
Planck Collaboration et al., 2015a, preprint, (arXiv:1502.01582)
Planck Collaboration et al., 2015b, preprint, (arXiv:1502.01589)
Pober J. C., et al., 2013, AJ, 145, 65
Pober J. C., et al., 2014, ApJ, 782, 66
Pober J. C., et al., 2015, ApJ, 809, 62
Presley M. E., Liu A., Parsons A. R., 2015, ApJ, 809, 18
Pritchard J. R., Loeb A., 2010, Phys. Rev. D, 82, 023006
Pritchard J. R., Loeb A., 2012, Reports on Progress in Physics, 75, 086901
Rogers A. E. E., Bowman J. D., 2008, AJ, 136, 641
Santos M. G., Cooray A., Knox L., 2005, ApJ, 625, 575
Shaver P. A., Windhorst R. A., Madau P., de Bruyn A. G., 1999, A&A, 345, 380
Sokolowski M., et al., 2015, Publ. Astron. Soc. Australia, 32, 4
Switzer E. R., Liu A., 2014, ApJ, 793, 102
Switzer E. R., et al., 2013, MNRAS, 434, L46
Thyagarajan N., et al., 2013, ApJ, 776, 6
Thyagarajan N., et al., 2015a, ApJ, 804, 14
Thyagarajan N., et al., 2015b, ApJ, 807, L28
Tingay S. J., et al., 2013, Publ. Astron. Soc. Australia, 30, 7
Trott C. M., Wayth R. B., Tingay S. J., 2012, ApJ, 757, 101
Valdés M., Evoli C., Mesinger A., Ferrara A., Yoshida N., 2013, MNRAS, 429, 1705
Vedantham H., Udaya Shankar N., Subrahmanyan R., 2012, ApJ, 745, 176
Vedantham H. K., Koopmans L. V. E., de Bruyn A. G., Wijnholds S. J., Ciardi B., Brentjens M. A., 2014, MNRAS, 437, 1056
Vedantham H. K., et al., 2015, MNRAS, 450, 2291
Visbal E., Loeb A., Wyithe S., 2009, J. Cosmology Astropart. Phys., 10, 30
Voytek T. C., Natarajan A., Jáuregui García J. M., Peterson J. B., López-Cruz O., 2014, ApJ, 782, L9
Wang X., Tegmark M., Santos M. G., Knox L., 2006, ApJ, 650, 529
Zaldarriaga M., 1997, Phys. Rev. D, 55, 1822
Zaldarriaga M., Furlanetto S. R., Hernquist L., 2004, ApJ, 608, 622
Zawada K., Semelin B., Vonlanthen P., Baek S., Revaz Y., 2014, MNRAS, 439, 1615
de Oliveira-Costa A., Tegmark M., Gaensler B. M., Jonas J., Landecker T. L., Reich P., 2008, MNRAS, 388, 247
van Haarlem M. P., et al., 2013, A&A, 556, A2